Statistical Mechanical Model of Topological Fluctuations and the Intermediate Phase in Binary Phosphate Glasses

Katelyn A. Kirchner[1], Mikkel S. Bødker[2], Morten M. Smedskjaer[2], Seong H. Kim[1,3], and John C. Mauro[1,*]

[1]*Department of Materials Science and Engineering, The Pennsylvania State University, University Park, Pennsylvania 16802, USA*

[2]*Department of Chemistry and Bioscience, Aalborg University, 9220 Aalborg, Denmark*

[3]*Department of Chemical Engineering, The Pennsylvania State University, University Park, Pennsylvania 16802, USA*

[*]*Corresponding Author:* jcm426@psu.edu

Abstract: Glasses are topologically disordered materials with varying degrees of fluctuations in structure and topology. This study links statistical mechanics and topological constraint theory to quantify the degree of topological fluctuations in binary phosphate glasses. Since fluctuations are a potential mechanism enabling self-organization, we investigated the ability of phosphate glasses to adapt their topology to mitigate localized stresses, e.g., in the formation of a stress-free intermediate phase. Results revealed the dependency of both glass composition and temperature in governing the ability of a glass network to relax localized stresses and achieve an ideal, isostatic state; also, the possibility of a second intermediate phase at higher modifier content was found.

I. Introduction

Designing new glass compositions requires accurate structural understanding; however, the complex chemical composition and disordered structure of glasses complicate achievement of this objective. As a result, most previous descriptions of glass structures and properties have only been in terms of their mean or expectation values. The understanding of spatial fluctuations, including fluctuations in glass structure and network topology, can offer a more complete description of a glass. Prior work by Kirchner *et al.* proposed a generalized approach for modeling topological fluctuations as a function of temperature and chemical composition through the use of statistical mechanics and topological constraint theory.[1] Such a model couples the composition-structure relations (from statistical mechanics) with the structure-property relations (through topological constraint theory) to optimize new glass compositions effectively.[2]

Structural and topological fluctuations directly impact several important glass properties. For example, Rayleigh scattering is a function of localized density fluctuations.[3-4] Also, the relaxation modes in a glass are dependent on atomic scale fluctuations;[5-8] crack propagation is affected by localized changes in bonding,[9] and nucleation and phase separation are also triggered by local fluctuations.[10-13] The scope of the current paper includes structural and topological fluctuations in binary phosphate glass systems.

Within the study of topological constraint theory, there is growing interest in the ability of a glass network to adapt its topology to achieve isostaticity in nominally overconstrained systems. In an overconstrained disordered network, the number of geometrically independent constraints exceeds the number of translational degrees of freedom of the atoms. Since the network is disordered, these rigid constraints are mutually incompatible. This incompatibility of the constraints leads to localized stresses, which, in turn, provide a thermodynamic driving force

for relaxation, i.e., to eliminate the localized stresses and create a stress-free network. The stresses from incompatible constraints can be eliminated either (a) via crystallization, i.e., through the imposition of geometric order, where geometrically independent (incompatible) constraints become dependent (compatible); or (b) via topological fluctuations that enable adaptation of the disordered network to reduce the number of incompatible constraints while maintaining a disordered structure. Hence, topological fluctuations can enable the atoms to self-organize into a stress-free state while maintaining a non-crystalline structure. These structural rearrangements relieve local stresses, driving the nominally overconstrained system back toward isostaticity.[14-15]

In the mean-field description of glass topology, a glass network is isostatic when the number of rigid constraints per atom, n, equals the number of translational degrees of freedom.[16] Hence, for a system in three-dimensional space, $\langle n \rangle = 3$ is the condition for achieving an isostatic network.[17] If $\langle n \rangle > 3$ the system is overconstrained and considered stress rigid due to the presence of mutually incompatible rigid constraints in the disordered glass network. If $\langle n \rangle < 3$ the system is underconstrained and contains floppy modes.[17]

In the original work by Phillips and Thorpe, the isostatic state was considered to occur at a single point;[18] however, in 1999, Boolchand *et al.* performed Raman scattering and temperature-modulated differential scanning calorimetry (MDSC) experiments, which concluded a finite width of isostatic compositions in which the system can maintain optimal stability. Boolchand coined this finite width the *intermediate phase* (IP).[14-15]

Within the glass community, there is a controversy surrounding the existence of this phenomenon. One such objection is the lack of a structural signature apparent in experimental results.[19] Lucas *et al.* hypothesized that the phase could be an artifact resulting from single

modulated frequency in the MDSC experiments.[20] However, subsequent computational evaluations showed a non-reversing heat flow independent of the modulation of frequency.[21] Further research is required to clarify the controversy regarding this topic. Previous work by Kirchner and Mauro has explored topological fluctuations and their impact on revealing more information about this proposed intermediate phase for arbitrary glass-forming systems.[22] This paper extends that work and applies the theory to binary phosphate systems.

Phosphate glasses are remarkable for their low glass transition temperatures, high thermal expansion coefficients, high rare earth solubility, and optical properties including high ultraviolet light transparency.[23-24] These properties make phosphate glasses attractive for applications in solid state lasers, biocompatible bone replacement materials, solid-state ionic devices, and glass-to-metal seals.[23-24] Previous work by Bødker *et al.* presents a statistical description of the compositional evolution of the mean structural units (Q^j-speciation) within phosphate glasses.[25] Here, we extend their work to explore the fluctuations in structural units and thereby the ability of glasses to rearrange.

This paper investigates the structural and topological fluctuations of binary phosphate glasses as a function of modifier concentration and temperature for five systems: $x$$Cs_2O$(1-$x$)$P_2O_5$, $x$$Na_2O$(1-$x$)$P_2O_5$, $x$$Li_2O$(1-$x$)$P_2O_5$, xMgO(1-x)P_2O_5, and xZnO(1-x)P_2O_5. We also consider the ability of the phosphate glass networks to adapt their topology to eliminate stresses, in order to study the origin of the intermediate phase experimentally reported in these glassy systems.[26]

II. Theory

Although glass-forming systems lack long-range order, the connectivity of the phosphate network is described by short-range structures, denoted by Q^j species, where j is the number of bridging oxygens (BO) bonded to the phosphorus atom.[27] Pure P_2O_5 is nominally composed exclusively of phosphate tetrahedra with three BOs and one double-bonded terminal oxygen (TO); therefore, this unit is denoted as Q^3. Addition of a modifier ion causes one BO to be converted to a non-bridging oxygen (NBO), where the NBO coordinates to modifier ions.[2] This new unit has two BOs and is denoted as Q^2. Due to electron delocalization, as the Q^3 unit becomes a Q^2 unit, the TO on the Q^3 unit also becomes an NBO.[23] The addition of more modifier ions follows this similar pattern from Q^3 to Q^2, Q^2 to Q^1, and Q^1 to Q^0.[23] These structural units are shown in Figure 1. The units themselves are considered to be bonded in a random manner throughout the network.[23]

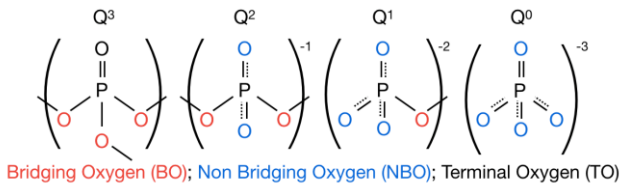

Figure 1. The four structural building blocks that constitute phosphate glasses.

The transition among Q^j species is based on the competition between entropy and enthalpy, which can be modeled using statistical mechanics. The probability of occupying site type i, where each site is considered a type of Q^j unit, with the m^{th} modifier atom is given by,[28-29]

$$p_{i,m} = \frac{(g_i - a_{i,m-1}) \exp\left(-\frac{H_i}{kT_f}\right)}{\sum_{i=1}^{\Omega} \sum_{j=o}^{m-1} (g_i - a_{i,j}) \exp\left(-\frac{H_i}{kT_f}\right)} \quad . \tag{1}$$

The entropic contribution to the bonding preferences is given by the $g_i - a_{i,m-1}$ prefactor, where g_i is the number of available network former sites of type i, and $a_{i,m-1}$ is the number of type i sites previously occupied after modifier $m-1$. The exponential term is the Boltzmann weighting factor, which accounts for the enthalpic contribution to the bonding statistics. H_i is the relative enthalpy change associated with occupying site type i, k is Boltzmann's constant, T_f is the fictive temperature of the glass, and the denominator normalizes the probability distribution. Due to the incorporation of the Boltzmann weighting factor, Eq. (1) yields a noncentral hypergeometric distribution of site occupation probabilities, thus providing a means for calculating the complete statistics of glass structure as a function of composition and fictive temperature.[29] Previous work by Bødker *et al.* has explored the mean Q^j speciation in binary phosphate glasses to fit the H_i values associated with each transition against experimental data.[25] This paper utilizes the enthalpy values from Bødker *et al.* as inputs for our statistical model investigating the topological fluctuations.

The topology of phosphate glasses is based on the structure and interactions of Q^j species, BO, NBO, and modifier ions ($M^{\theta+}$), where θ is the valance number. For the alkali ions (e.g., Li_2O, Na_2O, Cs_2O) $\theta = 1$ and for the divalent ions (e.g., MgO, ZnO) $\theta = 2$. Therefore the composition of phosphate system under exploration can be written as $x\mathrm{M}_{2/\theta}\mathrm{O}(1\text{-}x)\mathrm{P}_2\mathrm{O}_5$.

The number of rigid constraints in the network is based on counting the number of constraints per atom for the given network topology. To calculate the fraction of Q^j species per phosphorus atom, a scaling factor s is used. For the alkali phosphates, $x\mathrm{M}_2\mathrm{O}(1\text{-}x)\mathrm{P}_2\mathrm{O}_5$, the fraction of phosphorus atoms is

$$s = \frac{2-2x}{7-4x} \ , \tag{2}$$

and the fraction of alkali modifier cations is

$$M^{+}(x) = \frac{2x}{7-4x} \ . \quad (3)$$

where the denominator is the total number of atoms in the chemical formula.

For phosphates modified with divalent cations, xMO(1-x)P_2O_5, the fraction of phosphorus atoms is

$$s = \frac{2-2x}{7-5x} \ , \quad (4)$$

and the fraction of divalent modifying cations is

$$M^{2+}(x) = \frac{x}{7-5x} \ . \quad (5)$$

In the limit of infinite temperature, there is enough thermal energy to break any constraint, i.e., the system has zero rigid constraints per atom. As temperature decreases, more constraints become rigid. The total number of rigid constraints per atom is given by the sum of constraints that provide rigidity at the temperature of interest:[23]

$$n(x) = \sum n_c(x) \quad (6)$$

where $n_c(x)$ is the number of each type of constraint c. There are six types of constraints to consider within these phosphate systems: in order of decreasing strength, $\alpha > \beta > \gamma > \delta > \varepsilon > \zeta$. The α constraint represents the O-P-O angular constraint, given by,[23]

$$n_\alpha(x) = 3sQ^3(x) + 5s[Q^2(x) + Q^1(x) + Q^0(x)] \quad (7)$$

There are two linear constraints to consider; β is the P-O linear constraint given by,[23]

$$n_\beta(x) = 2BO(x) + NBO(x) \ . \quad (8)$$

Note that no constraints are counted at the TOs, as they are only bonded to one other atom and are hence not an integral part of the glassy network. The second linear constraint is γ, the $M^{\theta+}$ −O bond. The structure of the modifier ion and NBO bond depends on the concentration of modifier ions. At a critical cation concentration, x_{crit}, $M^{\theta+}$ begins to form corner or edge

sharing tetrahedra with NBO nearest neighbors.[23] This change in structure alters the number of constraints in the network. For Na^+, Li^+, Mg^{2+}, and Zn^{2+}, this critical modifier concentration is $x_{crit} = 0.2$.[23] Due to the large ionic radius of Cs^+, its threshold is found to be $x_{crit} = 0.17$.[30] The structural changes present above this threshold necessitate the use of a piecewise function for the γ constraint, given by,[23]

$$n_\gamma(x) = \begin{cases} \frac{2}{\theta} M^{\theta+}(x); \;\; 0 \le x \le x_{crit} \\ C_N M^{\theta+}(x - x_{crit}) + \frac{2}{\theta} M^{\theta+}(x_{crit}); \;\; x_{crit} < x \end{cases} \tag{9}$$

where C_N is the coordination number of the modifier ion to other network former atoms.

The remaining three types of constraints are all angular constraints. The P-O-P δ angular constraint occurs at each bridging oxygen (BO) given by,[23]

$$n_\delta(x) = BO(x) \, . \tag{10}$$

The P-O-$M^{\theta+}$ ε angular constraint incorporates the non-bridging oxygens (NBO) given by,[23]

$$n_\varepsilon(x) = \begin{cases} NBO(x); \;\; 0 \le x \le x_{crit} \\ 2NBO(x - x_{crit}) + n_\varepsilon(x_{crit}); \;\; x_{crit} < x \end{cases} , \tag{11}$$

and the O-$M^{\theta+}$-O ζ angular constraint is given by,[23]

$$n_\zeta(x) = \begin{cases} M^{\theta+}(x); \;\; 0 \le x \le x_{crit} \\ 5M^{\theta+}(x - x_{crit}) + n_\zeta(x_{crit}); \;\; x_{crit} < x \end{cases} . \tag{12}$$

Eqs. (7)-(12) can be substituted into Eq. (6) to calculate the total number of constraints per atom in the system.

The degree of topological fluctuations in the glass depends on both composition and thermal history. For a standard cooling rate of ~10 K/min, the fictive temperature T_f of the glass is equal to its glass transition temperature T_g, i.e., $T_f = T_g$. A polynomial fit from Bødker *et al.* approximates T_g as a function of x.[25] Preliminary testing confirmed that the accuracy of the

approximated T_g is insignificant in altering the calculation of the approximated intermediate phase or extent of fluctuations.

The intermediate phase represents a range of glass compositions having an ideal isostatic network. There are two boundaries that determine the width of isostatic compositions: the rigidity threshold and the stress threshold. The rigidity threshold represents the transition from a flexible to an isostatic network and it occurs when

$$\langle n \rangle = 3 \, , \tag{13}$$

where n is the number of constraints per atom and three is the dimensionality of space.

The stress threshold is the boundary between the isostatic region and the stressed-rigid regime. The ability of an overconstrained system to rearrange itself into a stress-free state, and hence yield an intermediate phase of nonzero width, is based on $P(n)$, the probability density of the rigidity distribution *n*. The stress transition is thus based on the probability of the system being able to rearrange its topology to achieve an average atomic rigidity less than or equal to 3. We denote this probability as f, which is given by

$$f = \int_0^3 P(n) \, dn \, . \tag{14}$$

Since different degrees of self-organization may be accessible to a given system, we define a threshold value, f_{thres}, which indicates the minimum value of f for which the system can adapt its network to eliminate localized stresses. The physical meaning of f_{thres} is to capture the adaptability of a glassy network to rearrange its configuration in response to localized stresses. As mentioned in the Introduction, these localized stresses result from mutually incompatible constraints in the glass network and provide a thermodynamic driving force for relaxation, i.e., to achieve a stress-free configuration. In other words, the condition $f = f_{thres}$ defines the point of the stress transition. If $f > f_{thres}$, the system can rearrange itself into a stress-free isostatic state,

but once $f < f_{thres}$, the stresses in the network are too high to fully relax, so the system remains in a stress-rigid state. The number of constraints at the stress transition is given by

$$n_{stress} = \langle\, n(x, f_{thres}) \,\rangle\,. \tag{15}$$

The width of the intermediate phase is the difference between the two boundaries established in Eq. (13) and Eq. (15). This width in terms of composition, w_x, is based on the difference between x_1, the composition at the rigidity percolation threshold $n = 3$, and x_2, the composition at n_{stress}, given by

$$w_x = x_2\,(\,n_{stress}, f_{thres}) - x_1\,(n = 3)\,. \tag{16}$$

Evidence of the IP has been experimentally confirmed through numerical studies,[31] analysis of finite size clusters,[32] MDSC,[15,33-35] and Raman scattering.[15,34-37] In one such experiment, Boolchand *et al.* used modulated DSC to investigate the intermediate phase present in sodium phosphate glasses.[26] Results concluded $w_x = 8.5$ mol %, with the rigidity transition occurring at $x_1 = 37.5$ mol % and the stress transition occurring at $x_2 = 46.0$ mol %.[26]

III. Results and Discussion

Previous work by Bødker *et al.* determined the mean predicted Q^j species as a function of modifier concentration, x.[25] By iterating over Eq. (1) we can calculate the standard deviation of each structure being present, and therefore determine the fluctuations of Q^j species as a function of x. We consider the structural speciation of the glass as having been frozen from the liquid state at $T_f = T_g$. The resulting concentration of Q^j species as a function of modifier concentration x is plotted in Figure 2. The fluctuations of the Q^j species is described using the standard

deviation (STD), as shown as error bars in Figure 2. The mean Q^j fractions are validated by NMR experimental results.[38-44] A clearer representation of the fluctuations is shown in Figure 3 by plotting STD as a function of x.

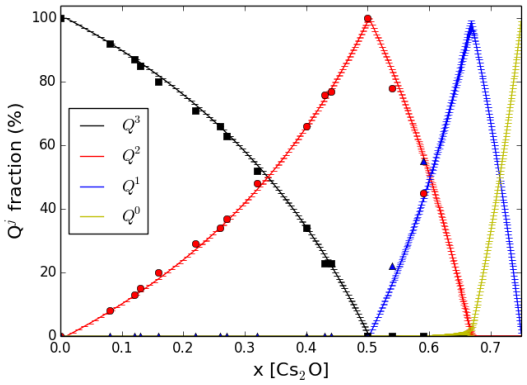

(a)

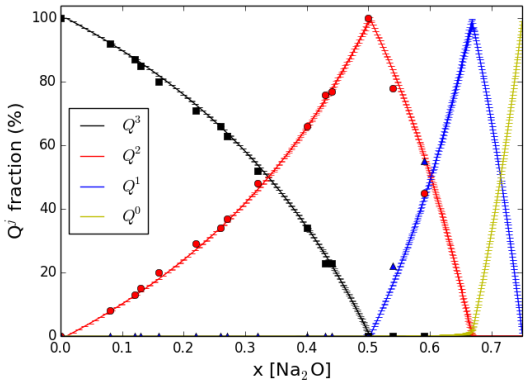

(b)

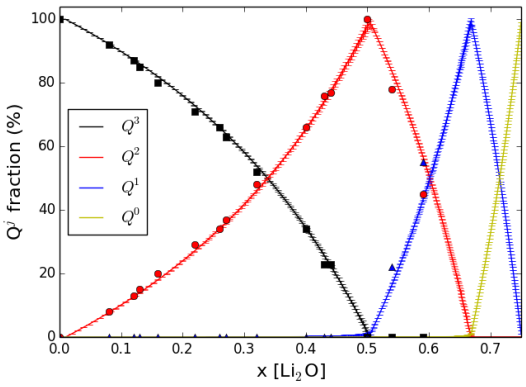

(c)

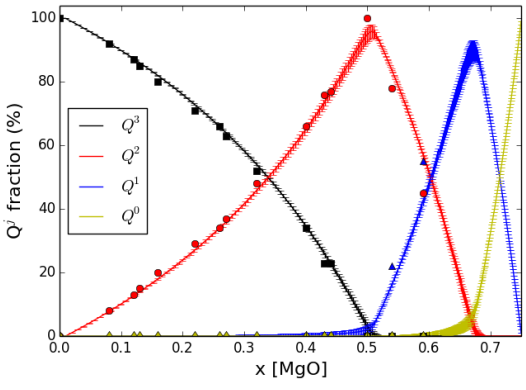

(d)

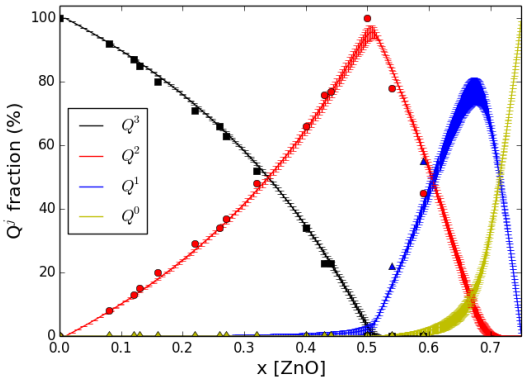

(e)

Figure 2. Validation of the mean Q^j species and representation of the fluctuation of Q^j species as a function of modifier concentration for (a) Cs_2O, (b) Na_2O, (c) Li_2O, (d) MgO, and (e) ZnO phosphate glasses. Errors bars represent the standard deviation of Q^j species over 3000 iterations, which are seen clearly at 400% enlargement. The symbols represent experimental NMR data, which validates the mean Q^j fraction.[38-44]

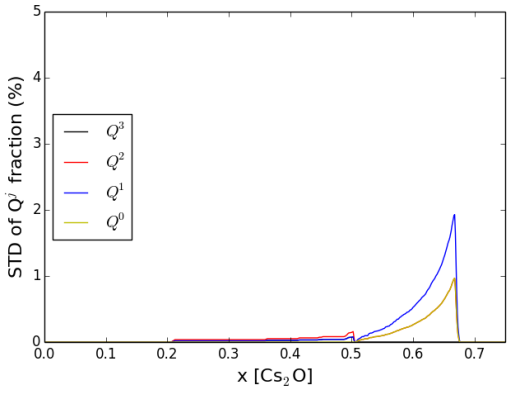

(a)

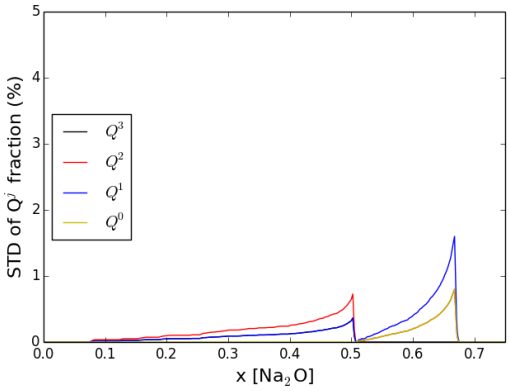

(b)

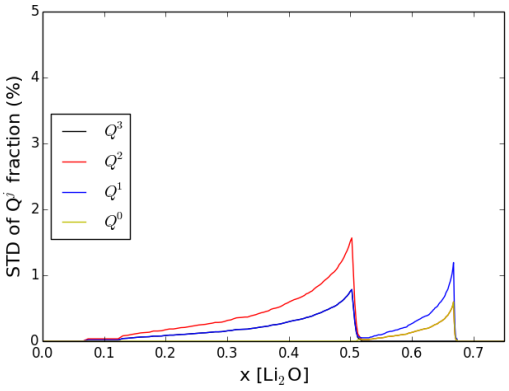

(c)

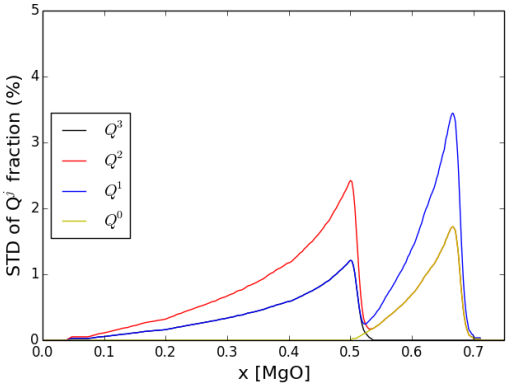

(d)

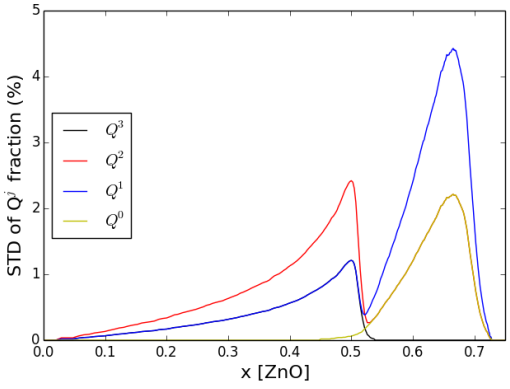

(e)

Figure 3. Standard deviation (STD) of Q^j species for (a) Cs_2O, (b) Na_2O, (c) Li_2O, (d) MgO, and (e) ZnO phosphate glasses over 3000 iterations.

Figures 2-3 reveal the impact of the competition between entropy and enthalpy dictating site occupation and the amount of fluctuations. Starting with low concentration of modifier, i.e., low *x* values, enthalpy dominates the speciation. Q^3 becoming Q^2 requires the least energy so that transition is preferred almost entirely, as shown by the small amount of fluctuations. As the population of Q^3 sites decreases, the contribution of entropy becomes more dominate allowing the transition from Q^2 to Q^1 to occur. The amount of fluctuations consequently increases. Once $x \sim 0.5$ mol fraction there are no more Q^3 species present in the network, therefore the modifiers can no longer form Q^2 and the amount of fluctuations dramatically decreases. Without Q^3 sites, the modifiers must form either Q^1 or Q^0 species. Q^1 and Q^0 species reduce the amount of BO, i.e., create shorter chains of P_2O_5 and reduce the rigidity of the network. With less rigidity, atoms can more easily rearrange, enabling the maximum amount of fluctuations in Q^j fraction. Once all Q^2 species are removed from the system, there is a singular transition available (e.g., Q^1 to Q^0), therefore the amount of fluctuations goes to 0.

Figure 2-3 also reveal the impact of modifier ion, more specifically presenting a correlation between decreasing cation size and increasing amount of structural fluctuations. Smaller alkali cations have smaller magnitude enthalpy values associated with each Q^j transition, i.e., the cations more easily rearrange, hence enabling a greater extent of fluctuations. Divalent modifiers have even smaller magnitude enthalpy values associated with each transition,[25] enabling an even larger extent of fluctuations.

Previous investigations with chalcogenides and oxide glasses show similar correlation between modifier cation size and smaller reversibility windows, where a proposed mechanism is topological fluctuations. These investigations have explored glasses with various bonding types, ionic-covalent (silicates),[45] covalent (Ge-Se),[46] and semi-metallic (Ge-Te-In-Ag).[47] Additionally, previous explorations in topological fluctuations have revealed that smaller magnitude enthalpy transitions enable a larger competition between entropy and enthalpy, enabling larger topological and structural fluctuations.[1]

With a known Q^j speciation, we can determine the number of each species per formula unit within $x\mathrm{M}_{2/\theta}\mathrm{O}(1\text{-}x)\mathrm{P}_2\mathrm{O}_5$ for both the monovalent ($\theta = 1$) and divalent ($\theta = 2$) modifier systems, as shown in Figure 4.

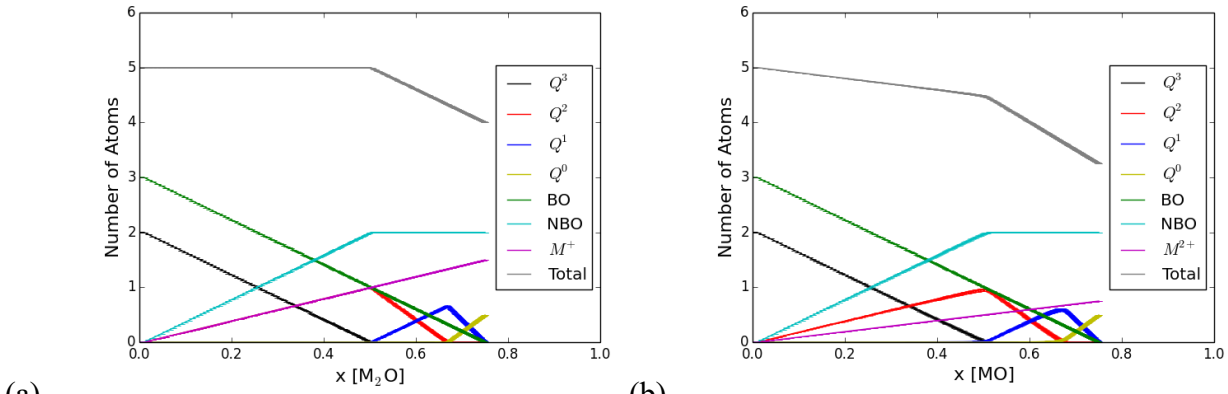

Figure. 4. The number of each network forming species per formula unit for (a) monovalent oxide phosphate glasses and (b) divalent oxide phosphate glasses.

Linking the results from Figure 4 and Eqs. (6)-(12) determines the mean value and amount of fluctuations of *n* as shown in the abstract image where the number of constraints per atom and the amount of fluctuations (i.e., the standard deviation of constraints) are plotted against the mole % of Na_2O. *n* is also temperature dependent, where the amount of rigid

constraints decreases with increasing temperature. To represent this impact of temperature, Figure 5 plots n for various types of constraints, where the ensemble is either fully rigid of fully flexible. This discrete counting of constraints is an approximation because for a given type of constraint, the ensemble can have partial rigidity, i.e., some occurrences can be rigid while others are flexible. In Figure 5, note that the kink at $x \sim 0.2$ occurs due to the piece wise functions of γ, ε, and ζ, as introduced in Section II.

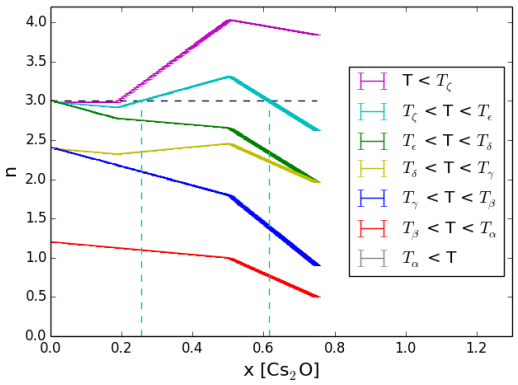

(a)

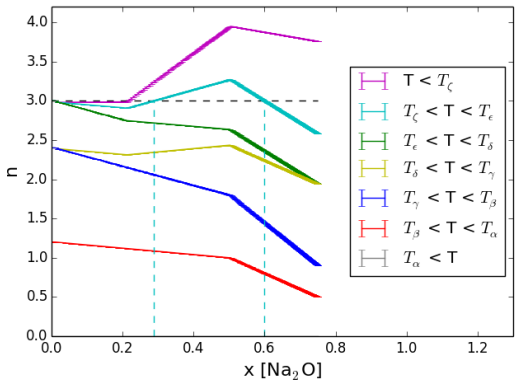

(b)

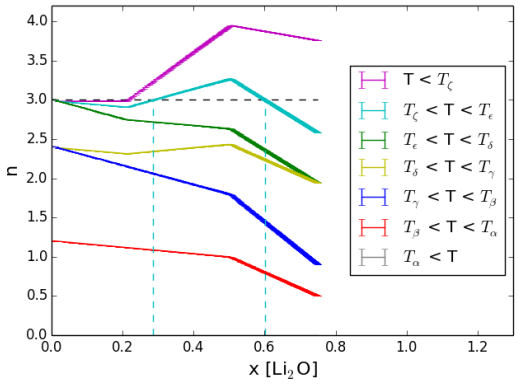

(c)

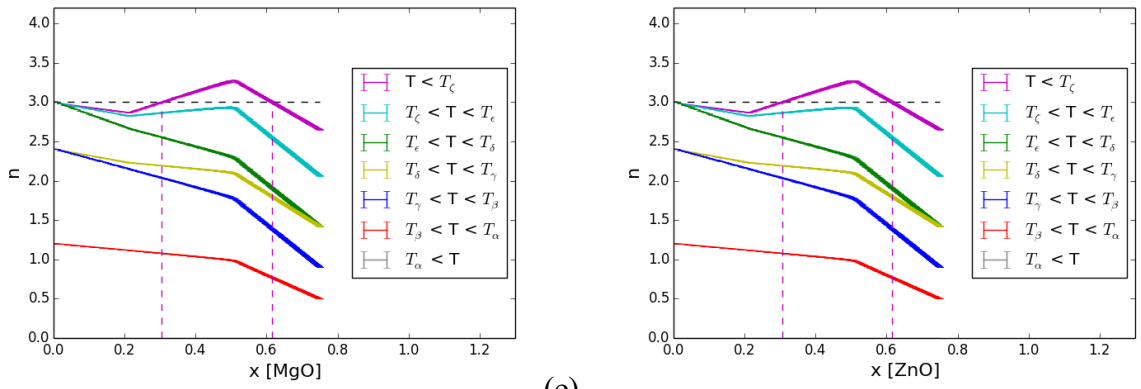

(d) (e)

Figure 5. The mean value and fluctuations in the number of constraints per atom, n, as a function of composition and temperature for (a) Cs_2O, (b) Na_2O, (c) Li_2O, (d) MgO, and (e) ZnO phosphate glasses. The fluctuations are represented as the error bars, which is the standard deviation of n (number of rigid constraints per atom) over 3000 iterations.

The boundaries of the intermediate phase can be deduced based on the temperature regime in Figure 5, where the number of atomic constraints crosses the rigidity percolation threshold at $n = 3$. Thus, for the monovalent modifiers in Figures 5(a)-(c), the relevant temperature regime is represented by the cyan colored plot where $T_\zeta < T < T_\varepsilon$. For the divalent modifiers in Figure 5(d)-(e), the temperature range of interest is represented by the magenta colored plot where $T < T_\zeta$.

Wherever the number of constraints per atom crosses $n = 3$, the system passes through a rigidity transition, inferring that an intermediate phase could be present. One of the interesting results from Figure 5 is the possible existence of a second intermediate phase at high modifier concentrations. Prior experimental studies have focused their investigations around 28-50 mol % modifier oxide.[15,26,31-37] However, in Figure 5 there appears to be a second IP phase around 60

mol % in both the monovalent and divalent systems. Future experimental results will be necessary to investigate this possible second IP.

To quantify the widths of these intermediate phases, the value of f_{thres} is necessary, which we can determines using the modulated DSC results from Boolchand *et al.* for the sodium phosphate system.[26] From Figure 5(b), our model found the rigidity transition to be at $x_1 \approx 28$ mol %. With an assumed width of $w_x = 8.5$ mol %, the stress transition must then occur at $x_2 \approx 36.5$ mol %, which marks the modifier composition of n_{stress} and f_{thres}. At x_2 the standard deviation $\sigma = 1.2 * 10^{-4}$ and the mean number of constraints $\mu = 3.103$. Using Eq. (14), $f_{thres} \approx 0$. The f_{thres} calculated from our model is therefore too small to physically represent an intermediate phase as wide as that reported by Boolchand *et al.*[26] Additionally, our model underestimates x_1 and x_2 compared to the corresponding results from Boolchand *et al*.[26]

These inconsistences point toward a need for another physical response contributing to the experimentally observed intermediate phase width. The modulated DSC results from Boolchand *et al.* were obtained at a scan rate of 3°C/min, modulation amplitude of ±1°C, and modulation time of 100 s.[26] On the other hand, our model for isostaticity assumes constant temperature. Therefore, we hypothesize that the underestimation of x_1 and x_2 comes from neglecting the modulation over a wide range of temperatures. To properly represent the experimental results, our model must incorporate the continuous modulation of temperature that is present in the experimental results.

Specifically, our underestimation may be a result of assuming discrete constraint onset functions. As the temperature of the $T_\zeta < T < T_\varepsilon$ system increases, constraints break, hence transitioning to $T_\delta < T < T_\zeta$. This continuous transition will shift the *x*-intercept with $n = 3$ to higher modifier concentrations. Higher *x* values also correspond with larger amount of

fluctuations, enabling a wider IP. Therefore, the proposed rationale for the discrepancy between our model and the results from Boolchand *et al.* is that our model fails to incorporate the continuous modulation of temperature.

Without a correlated f_{thres} value, the IP width must be represented in terms of an arbitrary allowed standard deviation, as shown in Figure 6. Note that the values for the IP width are very small because the model is underestimating the *x* value, and therefore calculating the IP width at a composition with smaller amounts of fluctuations. Similar to Figure 3, Figure 6 confirms that smaller cation atomic radii enable larger extents of topological fluctuations. With more probabilistic atomic rearrangement comes larger intermediate phase widths.

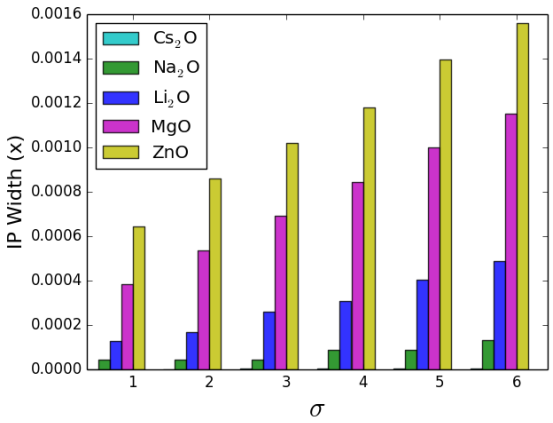

Figure 6. The IP width surrounding $x \approx 0.2 - 0.3$ in units of the mole fraction *x* versus the allowed number of standard deviations, σ, shown for varying modifier cations in binary phosphate glasses. Note the IP width for Cs_2O is $\sim 5^{-6}$.

IV. Conclusions

This paper has established a statistical mechanical model to measure topological fluctuations and the ability of networks to rearrange in binary phosphate glasses. The competition between entropy and enthalpy of the network dictates speciation and the amount of

fluctuations. The size and charge of the modifier ion alters this competition since the smaller cation radius, the lower the enthalpy associated with changes in Q^j speciation, and therefore the larger the extent of topological fluctuations and a larger IP width. To model the intermediate phase, a key conclusion is the necessity to incorporate a continuous change in temperature as well as the current continuous change in modifier concentration. Future work will incorporate the continuous modulation of temperature that is present in the experimental results to improve the accuracy of the phosphate statistical model. Future work will also continue to refine the model by comparing other glass forming systems with their experimentally observed intermediate phases. The simulation results also reveal the presence of a second intermediate phase. Future experimental investigations will need to be conducted at ~ 60 mol % of modifier oxide to investigate the presence and impact of this second IP.

V. Acknowledgement: We would like to thank Punit Boolchand for his invaluable guidance and providing his preprint manuscript experimentally exploring the intermediate phase in sodium phosphate glasses. M.M.S. acknowledges funding from the Independent Research Fund Denmark (Grant No. 7017-00019). J.C.M. acknowledges funding from the U.S. National Science Foundation (CMMI 1762275).

VI. References

[1] Kirchner, K. A; Kim, S. H.; Mauro, J. C. Statistical mechanics of topological fluctuations in glass-forming liquids. *Phys. A* **2018,** *510*, 787-801.

[2] Wright, A. C.; Shakhmatkin, B. A.; Vedishcheva, N. M. The chemical structure of oxide glasses: A concept consistent with neutron scattering studies? *Glass Phys. Chem*. **2001,** *27*, 97−113.

[3] Mauro, J. C.; Uzun, S. S.; Bras, W.; Sen, S.; Nonmonotonic evolution of density fluctuations during glass relaxation. *Phys. Rev. Lett.* **2009,** *102*, 155506.

[4] Mauro, J. C. Effect of fragility on relaxation of density fluctuations in glass. *J. Non-Cryst. Solids* **2011**, *357*, 3520-3523.

[5] Ellison, A.; Cornejo, I. A. Glass substrates for liquid crystal displays. *Int. J. Appl. Glass. Sci.* **2010,** *1*, 87-103.

[6] Vargheese, K. D.; Tandia, A.; Mauro, J. C. Origin of dynamical heterogeneities in calcium aluminosilicate liquids. *J. Chem. Phys.* **2010**, *132*, 194501.

[7] Welch, R. C.; Smith, J. R.; Potuzak, M.; Guo, X.; Bowden, B. F.; Kiczenski, T. J.; Allan, D. C.; King, E. A.; Ellison, A. J.; Mauro, J. C. Dynamics of glass relaxation at room temperature. *Phys. Rev. Lett.* **2013,** *110*, 265901.

[8] Zheng, Q.; Mauro, J. C. Variability in the relaxation behavior of glass: Impact of thermal history fluctuations and fragility. *J. Chem. Phys.* **2017,** *146*, 074504.

[9] Wang, B.; Yu, Y.; Wang, M.; Mauro, J. C.; Bauchy, M. Nanoductility in silicate glasses is driven by topological heterogeneity. *Phys. Rev. B* **2016,** *93*, 064202.

[10] Okabe, I.; Tanaka, H.; Nakanishi, K. Structures and phase transitions of amorphous ices. *Phys. Rev. E* **1996,** *53*, 2638-2647.

[11] Micoulaut M.; Naumis, G. G. Glass transition temperature variation, cross-linking and structure in network glasses: A stochastic approach. *Europhys. Lett.* **1999,** *47*, 568-574.

[12] Dargaud, O.; Cormier, L.; Menguy, N.; Patriarche, G. Multi-Scale structuration of glasses: Observations of phase separation and nanoscale heterogeneities in glasses by Z-contrast scanning electron transmission microscopy. *J. Non-Cryst. Solids* **2012,** *358*, 1257-1262.

[13] Kim, D. H.; Kim, W. T.; Park, E. S.; Mattern, N.; Eckert, J. Phase separation in metallic glasses. *Prog. Mater. Sci.* **2013,** *58*, 1103-1172.

[14] Boolchand, P.; Georgiev, D. G.; Goodman, B. Discovery of the intermediate phase in chalcogenide glasses. *J. Optoelectron. Adv. M.* **2001,** *3*, 703-720.

[15] Selvanathan, D.; Bresser, W. J.; Boolchand, P.; Goodman, B. Thermally reversing window and stiffness transitions in chalcogenide glasses. *Solid State Commun.* **1999,** *111*, 619-624.

[16] Phillips, J. C. Topology of covalent non-crystalline solids I: Short-range order in chalcogenide alloys. *J. Non-Cryst. Solids* **1979,** *34*, 153-181.

[17] Thorpe, M. F. Continuous deformations in random networks. *J. Non-Cryst. Solids* **1983,** *57*, 355-370.

[18] Phillips, J. C.; Thorpe, M. F. Constraint theory, vector percolation and glass formation. *Solid State Commun.* **1985,** *53*, 699-702.

[19] Zeidler, A.; Salmon, P. S.; Whittaker, D. A.J.; Pizzey, K. J.; Hannon, A. C. Topological ordering and viscosity in the glass-forming Ge-Se system: The search for a structural or dynamical signature of the intermediate phase. *Front. Mater.* **2017,** *4*, 1-15.

[20] Lucas, P.; King, E. A.; Gulbiten, O.; Yarger, J. L.; Soignard, E.; Bureau, B. Bimodal phase percolation model for the structure of Ge-Se glasses and the existence of the intermediate phase. *Phys. Rev. B* **2009,** *80*, 214114.

[21] Guo, X.; Mauro, J. C.; Allan, D. C.; Yue, Y. On the frequency correction in temperature-modulated differential scanning calorimetry of the glass transition. *J. Non-Cryst. Solids* **2012,** *358*, 1710-1715.

[22] Kirchner, K. A.; Mauro, J. C. Statistical mechanical model of the self-organized intermediate phase in glass-forming systems with adaptable network topologies. *Front. Mater.* **2019,** *6*, 1-7.

[23] Hermansen, C.; Mauro, J. C.; Yue, Y. A model for phosphate glass topology considering the modifying ion sub-network. *J. Chem. Phys.* **2014,** *140*, 154501.

[24] Click, C. A.; Brow, R. K.; Alam, T. M. Properties and structure of cesium phosphate glasses. *J. Non-Cryst. Solids* **2002,** *311*, 294-303.

[25] Bødker, M. S.; Mauro, J. C.; Goyal, S.; Youngman, R. E.; Smedskjaer, M. M. Predicting Q-speciation in binary phosphate glasses using statistical mechanics. *J. Phys. Chem. B* **2018,** *122*, 7609-7615.

[26] Mohanty, C.; Mandal, A.; Gogi, V.; Chen, P.; Novita, D.; Chbeir, R.; Bauchy, M.; Micoulaut, M.; Boolchand, P. Linking melt dynamics with topological phases and molecular structure of sodium phosphate glasses from calorimetry, Raman scattering and infrared reflectance. *Front. Mater.* **2019,** *6*, 1-20.

[27] Brow, R. K. Review: The structure of simple phosphate glasses. *J. Non-Cryst. Solids* **2000,** *263-264*, 1-28.

[28] Mauro, J. C. Statistics of modifier distributions in mixed network glasses. *J. Chem. Phys.* **2013,** *138*, 12A522.

[29] Mauro, J. C.; Smedskjaer, M. M. Statistical mechanics of glass. *J. Non-Cryst. Solids* **2014,** *396*, 41-53.

[30] Hermansen, C.; Rodrigues, B. P.; Wondraczek, L.; Yue, Y. An extended topological model for binary phosphate glasses. *J. Chem. Phys.* **2014,** *141*, 244502.

[31] Thorpe, M. F.; Jacobs, D. J.; Chubynsky, M. V.; Phillips, J. C. Self-organization in network glasses. Part II. Chalcogenide and organic semiconductors. *J. Non-Cryst. Solids* **2000,** *266-269*, 859-866.

[32] Micoulaut, M.; Phillips, J. C. Rings and rigidity transitions in network glasses. *Phys. Rev. B* **2003,** *67*, 1042041-1042049.

[33] Boolchand, P.; Georgiev, D. G.; Goodman, B. Discovery of the intermediate phase in chalcogenide glasses. *J. Optoelectron. Adv. M.* **2001,** *3*, 703-720.

[34] Novita, D. I.; Boolchand, P.; Malki, M.; Micoulaut, M. Fast-Ion conduction and flexibility of glassy networks. *Phys. Rev. Lett.* **2007,** *98*, 195501.

[35] Selvanathan, D.; Bresser, W. J.; Boolchand, P. Stiffness transitions in Si_xSe_{1-x} glasses from Raman scattering and temperature-modulated differential scanning calorimetry. *Phys. Rev. B* **2000,** *61*, 15061-15076.

[36] Boolchand, P.; Feng, X.; Bresser, W. J. Rigidity transitions in binary Ge-Se glasses and the intermediate phase. *J. Non-Cryst. Solids* **2001,** *293-295*, 348-356.

[37] Wang, Y.; Wells, J.; Georgieve, D. G.; Boolchand, P. Sharp rigid to floppy phase transition induced by dangling ends in a network glass. *Phys. Rev. Lett.* **2001,** *87*, 1855031-1855034.

[38] van Wüllen, L.; Eckert, H.; Schwering, G. Structure−property correlations in lithium phosphate glasses: New insights from 31P ↔ 7Li double-resonance NMR. *Chem. Mater.* **2000,** *12*, 1840−1846.

[39] Alam, T. M.; Brow, R. K. Local structure and connectivity in lithium phosphate glasses: A solid-state 31P MAS NMR and 2D exchange investigation. *J. Non-Cryst. Solids* **1998,** *223*, 1−20.

[40] Brow, R. K.; Kirkpatrick, R. J.; Turner, G. L. The short range structure of sodium phosphate glasses I. MAS NMR studies. *J. Non- Cryst. Solids* **1990,** *116*, 39−45.

[41] Strojek, W.; Eckert, H. Medium-range order in sodium phosphate glasses: A quantitative rotational echo double resonance solid state NMR study. *Phys. Chem. Chem. Phys.* **2006,** *8*, 2276-2285.

[42] Click, C. A.; Brow, R. K.; Alam, T. M. Properties and structure of cesium phosphate glasses. *J. Non-Cryst. Solids* **2002,** *311*, 294−303.

[43] Fayon, F.; Massiot, D.; Suzuya, K.; Price, D. L. 31P NMR study of magnesium phosphate glasses. *J. Non-Cryst. Solids* **2001,** *283*, 88−94.

[44] Walter, G.; Vogel, J.; Hoppe, U.; Hartmann, P. Structural study of magnesium polyphosphate glasses. *J. Non-Cryst. Solids* **2003,** *320*, 210−222.

[45] Micoulaut, M. Amorphous materials: Properties, structure, and durability: Constrained interactions, rigidity, adaptative networks, and their role for the description of silicates. *Am. Mineral.* **2008,** *93*, 11-12.

[46] Bhosle, S.; Gunasekera, K.; Chen, P.; Boolchand, P.; Micoulaut, M.; Massobrio, C. Meeting experimental challenges to physics of network glasses: Assessing the role of sample homogeneity. *Solid State Commun.* **2011,** *151*, 1851-1855.

[47] Varma, G.; Das, C.; Asokan, S. Evidence of an intermediate phase in a quaternary Ag bearing telluride glass system using alternating DSC. *Solid State Commun.* **2014,** *177*, 108-112.

VII. TOC Image